Journal of Zhejiang University-SCIENCE A (Applied Physics & Engineering)
ISSN 1673-565X (Print); ISSN 1862-1775 (Online)
www.zju.edu.cn/jzus; www.springerlink.com
E-mail: jzus@zju.edu.cn

Use of bionic inspired surfaces for aerodynamic drag reduction on motor vehicle body panels

Xiao-wen SONG†, Guo-geng ZHANG, Yun WANG, Shu-gen HU

(*Department of Mechanical Engineering, Zhejiang University, Hangzhou 310027, China*)

†E-mail: songxw@zju.edu.cn

Received Dec. 14, 2010; Revision accepted Apr. 19, 2011; Crosschecked June 21, 2011

Abstract: Inspired by the successful applications of biological non-smoothness, we introduced bionic non-smooth surfaces as appendices into vehicle body design, aiming to further reduce aerodynamic drag. The size range of the non-smooth units with pits and grooves was determined according to our analysis with the mechanisms underlying non-smooth unit mediated aerodynamic drag reduction. The bionic non-smooth units reported here were designed to adapt the structure of a given vehicle body from the point of boundary layer control that reduces the burst and the loss of turbulent kinetic energy. The engine cover lid and vehicle body cap were individually treated with the non-smooth units, and the treated vehicles were subjected to aerodynamic drag coefficient simulation tests using the computational fluid dynamics (CFD) analysis method. The simulation results showed that, in comparison with smooth surfaces, properly designed non-smooth surfaces can have greater effects on drag reduction. The mechanism underlying drag reduction mediated by non-smooth surfaces was revealed by further analyses, in which the effects of non-smooth and smooth surfaces were directly compared.

Key words: Computational fluid dynamics (CFD), Bionics, Non-smooth surface, Aerodynamic drag reduction, Vehicle body
doi:10.1631/jzus.A1000505 **Document code:** A **CLC number:** U46; TB4

1 Introduction

The air resistance of a high-speed vehicle is mainly determined by the aerodynamic drag coefficient. Design with streamlined body has been a classical method to reduce the aerodynamic drag, and is still dominating vehicle design today. In addition, a number of studies have revealed that the aerodynamic drag can be further reduced by regional optimization. Singh *et al.* (2005) achieved drag reduction by optimizing the flow separation on vehicle body surfaces, whereas Fu and Cai (1998) proposed to improve the aerodynamic performance by placing a wind-resistant board at the lower-front body and attaching a flow-round slat in the back region of vehicle. Salari and co-workers (2006) observed reduced aerodynamic resistance in a truck model by using uniform air injection device in the rear of the truck. By installing turbulence break-up devices, Koike *et al.* (2004) were able to accomplish a reduced body drag. Gu *et al.* (2008) indicated that installation of gas injection device in the rear turbulence center of a car improves the aerodynamic performance. Nisugi *et al.* (2004) demonstrated drag reduction by adjusting the flow velocity of the injection device according to the feedback from the rear eddy flow.

Since streamline body design and regional optimization have been extensively explored, further aerodynamic drag reductions by using these two approaches will be limited. Therefore, it is necessary to develop additional approaches in order to overcome the current bottleneck in the study of vehicle aerodynamic drag reduction. For that reason, the bionic surface based approach has received a great deal of attention. Inspired by the successful application of biological non-smoothness, including the use of biomimetic structures in reducing the drag of furrow

© Zhejiang University and Springer-Verlag Berlin Heidelberg 2011

opener (Tong *et al.*, 2009), we previously reported the use of non-smooth surfaces as appendix on the vehicle body to reduce the aerodynamic drag (Song *et al.*, 2010).

Up to now, the effects of non-smooth surfaces on motor vehicle drag reduction have not been well studied. However, the effects of non-smooth surfaces on drag reduction, in comparison with smooth surface, in other areas have been extensively studied. For example, in the blunt-based flight vehicle, Whitmore and Naughton (2002) reported a net drag reduction by introducing roughness to the fore-body skin using micro-machined surface overlays. Fransson *et al.* (2006) suggested an approach aiming to maximize the time of boundary layer laminar by forcing small optimal perturbations. The results of their wind-tunnel experiments showed that the use of passive control technique, such as placing suitably designed roughness elements on the skin, can reduce the viscous drag probably by delaying the transition to turbulence. Gad-el-Hak (2006) pointed out that the proper use of compliant coating as a potential method to favorably interfere with the wall-bounded flow as it can affect laminar-to-turbulence transition, control boundary layer separation, modulate flow-induced noise, or alter skin friction drag in both laminar and turbulent flows.

The existing experimental and analytical studies indicate the prospective application of non-smooth surface with optimal physical properties in drag reduction. However, many technical obstacles still remain. As pointed out by Choi (2006), a major challenge in drag reduction is how to modify the organized structures of various shapes efficiently as the shape of the roughness elements is critical in stabilizing laminar flow and a slight change in shape may result in a completely different flow pattern. The study reported here is aiming to obtain efficient drag reduction using bionic non-smooth surface based approach. After analyzing the mechanisms underlying non-smooth surface mediated drag reduction, the bionic non-smooth units were designed as described below. The feasibility of aerodynamic drag reduction by the bionic non-smooth surfaces on vehicle body and its influence on the whole body aerodynamic characteristics were also investigated.

2 Design of bionic non-smooth units

Based on the studies with the shark's groove-like non-smooth surfaces, Walsh *et al.* (1989) found that aircraft with small grooves on its surface can significantly reduce the frictional drag at boundary layer. This promoted the application of bionic non-smooth surfaces in fluid drag reduction, and sparked a series of follow-up studies focusing on aerospace, seafaring, and military applications, as well as on soil mechanics, to reduce soil adhesion and friction in China. However, no study regarding the effects on bionic non-smooth surfaces to the aerodynamic resistance of motor vehicle body has yet been reported.

After studying the head and body pelage from 23 species of Western Australia bats, Bullen and McKenzie (2008) found that, in the species utilizing high-speed flight, the riblet non-smooth surfaces may contribute to the observed 10% frictional resistance reduction on the head and body skin areas. To study the effect of surface shape on frictional resistance, Bourisli and Al-Sahhaf (2008) analyzed the friction coefficient and velocity by a series of simulation tests using grooves in three different shapes, including square, triangle, and semi-circle. The results showed that all three non-smooth surfaces gave less resistance compared with smooth surfaces, and the square groove provided the greatest drag reduction. Using digital simulation technology, EI-Samni *et al.* (2005; 2007) were able to adjust the pressure gradient to stabilize the mass flow on rib-like non-smooth surfaces with different rib structures and inter-rib spaces. This system was used to optimize the geometric relationships between rib structures and inter-rib space in relation to drag reduction, and a maximal 11% drag reduction was obtained in these studies. Ren *et al.* (2005) included the bionic non-smooth surface consideration in the design of spinning surface. Smooth surface and non-smooth surfaces bearing various sizes of convex hulls, pits, ribs, and other types of non-smoothness were subjected to low speed, subsonic, and supersonic wind tunnel tests. The results showed that all the tested non-smooth surfaces gave reduced resistance and the highest drag reduction rate was approximately 5%. Zhou *et al.* (2006) studied the non-smooth surface of the pigeon feather. Placement

of pit-containing man-constructed non-smooth surfaces on the back of revolving body results as much as 16.56% drag reduction measured by simulation testing.

The aforementioned studies regarding the non-smooth surfaces and aerodynamic drag reduction serve as an excellent reference point for the design of non-smooth units on motor vehicles. Song *et al*. (2010) and Zhang (2010) attempted to incorporate the non-smooth surface idea into the motor vehicle body shape design, focusing on the non-smooth surfaces containing the units of pits and grooves illustrated in Fig. 1. As shown in Figs. 1a and 1b, the units are defined as uniformly distributed pits. The vertical distance of each unit, marked as u, is *L*, the horizontal distance between units is *S*, the height (or depth) of each unit is *H*, and the width of each unit is *D*. Also Figs. 1c and 1d are the units containing uniformly distributed grooves, of which the horizontal distance, the width, and the height are labeled as *s*, *d*, and *h*, respectively.

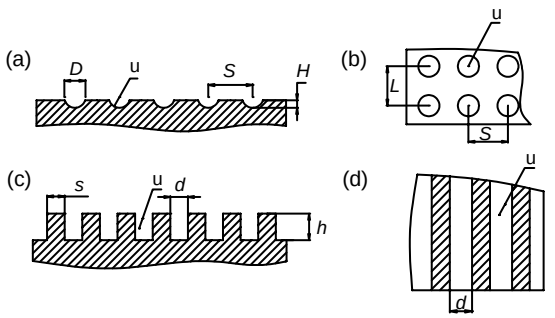

Fig. 1 Structure and distribution of the units
(a) and (b) Side- and top-views of uniformly distributed pits; (c) and (d) Side- and top-views of uniformly distributed grooves

To elucidate the mechanisms underlying the non-smooth surface mediated drag reduction, Sirovich and Karlsson (1997) introduced a V-shape groove in their wind tunnel tests to achieve the drag reduction. They found that the observed drag reduction is accompanied by reduced turbulent energy dissipation, suggesting a reduction in turbulent energy dissipation could be a mechanism used by the non-smooth surface approach. After synthesizing the published studies, Zhang (2007) speculated that bionic non-smooth surface mediates drag reduction by controlling the boundary layer, which subsequently reduces the frequency of burst and turbulent kinetic energy dissipation. Although lacking definitive evidence, this speculation still provides a useful guidance in practice.

According to the previous studies, in order to prevent bursts to occur and to achieve drag reduction, the height or depth of non-smooth units should be smaller than the distance between the body surfaces and the outermost part of the boundary layer, also known as the logarithmic law layer.

The movement of the airflow on the surface of the vehicle body is greatly influenced by the flowing conditions of the near boundary area, which contains three layers, namely, the viscous sub-layer, the buffer layer, and the logarithmic law layer. Here we refer this as a three-layer model. The space outside the near boundary area is called core zone or outer zone, where the flow is absolutely turbulent. In order to mathematically describe the flow state of the viscous sub-layer and the logarithmic law layer, two dimensionless parameters, the speed u^+ and the distance y^+, are introduced as follows (Wang, 2004):

$$\begin{cases} u^+ = u / u_\tau, \\ y^+ = (\Delta y / \nu)\sqrt{\tau_w / \rho}, \end{cases} \tag{1}$$

where u represents the time-average velocity of the airflow, u_τ is the friction velocity of the airflow near boundary area, Δy is the distance to the boundary, ν is the kinematic viscosity of the airflow, τ_w is the shear stress within the near boundary airflow, ρ is the density of the airflow, and $u_\tau=(\tau_w/\rho)^{1/2}$.

Studied with a simplified two-layer model, in which the buffer layer is not separately defined, Versteeg and Malalasekera (1995) found that $y^+=11.63$ is a dividing point between the viscous sub-layer and the logarithmic law layer. If the volume control nodes adjacent to the boundary meet $y^+\leq 11.63$, the control nodes are thought to be within the viscous sub-layer. In contrast, when $y^+>11.63$, the nodes are within the logarithmic law layer. The size of the interface between the logarithmic law layer and the core zone depends on the value of Reynolds number. According to Wang (2004), the volume control node is in the core zone when $y^+>300$. On the other hand, Fluent User's Guide (Fluent Inc., 2006) indicated that the volume control node is in the core zone when $y^+>500$. As mentioned above, in order to reduce the frequency of burst, the height or depth of body surface units

should be smaller than the distance between the body surface and the logarithmic law layer. To validate whether this rule applies to all the cases of drag reduction, the space of the logarithmic law layer used in this study covers a wide range within $11.63<y^+<116.3$ for the purpose of designing the size of non-smooth units.

The shear stress τ_w near the boundary area is given (Versteeg and Malalasekera, 1995):

$$\tau_w = \rho C_\mu^{1/4} k_P^{1/2} u / u^+, \tag{2}$$

where C_μ is the variable related to strain rate, k_P is the turbulent kinetic energy of node P, u is the time-average velocity of node P, and u^+ is the dimensionless parameter mentioned before.

Substituting Eq. (1) into Eq. (2), Eq. (2) can be simplified as

$$\tau_w = \rho k_P C_\mu^{1/2}, \tag{3}$$

where the turbulent kinetic energy $k_P=3/2(uI)^2$, the turbulence intensity $I=0.16Re^{-1/8}$ and Re is the Reynolds number.

The air density $\rho=1.293$ kg/m^3. The kinematic viscosity $\nu=1.589\times10^{-5}$ m^2/s. When the wind velocity $u=30$ m/s, the distance Δy between the boundary and the control node P in the logarithmic law layer can be given as

$$11.63\nu / \sqrt{\tau_w / \rho} < \Delta y < 116.3\nu / \sqrt{\tau_w / \rho}, \tag{4}$$

also satisfied as

$$\begin{cases} \Delta y > 3.14352\times10^{-5} Re^{1/8} C_\mu^{-1/4}, \\ \Delta y < 3.14352\times10^{-4} Re^{1/8} C_\mu^{-1/4}. \end{cases} \tag{5}$$

Because the fluid of viscous sub-layer is almost a laminar flow, the rotating air in the boundary between the viscous sub-layer and the logarithmic law layer is little enough to be ignored. Then the variable C_μ is given as (Wang, 2004):

$$C_\mu = \frac{1}{4+\sqrt{6}\cos\Phi\sqrt{E_{ij}E_{ij}}\,k/\varepsilon}, \tag{6}$$

where k and ε are the turbulent kinetic energy and turbulent kinetic energy dissipation rate, respectively, $\Phi = \frac{1}{3}\cos^{-1}[\sqrt{6}E_{ij}E_{jr}E_{rj}/(E_{ij}E_{ij})^{1/2}]$, and $E_{ij} = \frac{1}{2}\left(\frac{\partial u_i}{\partial x_j} + \frac{\partial u_j}{\partial x_i}\right)$. i, j, and r here are the markers defined by the tensor index convention with the value of 1, 2, and 3 as described by Wang (2004).

Based on the above analysis, the distance Δy between the boundary and the control node within the logarithmic law layer, which is also the distance from vehicle body surface to the node within the logarithmic law layer, can be determined according to the value of C_μ. However, it is difficult to solve the value of variable C_μ in practice, and it changes little on the range of vehicle body surfaces. Thus, the thickness of the boundary layer on the engine cover lid or body cap can be estimated by the calculation of turbulent boundary layer thickness on a plate.

The velocity of airflow on a plate does not change in any direction, which means $\partial u_i/\partial x_i\approx0$ and $\partial u_j/\partial x_i\approx0$, so $C_\mu\approx0.25$. Then according to Eq. (5), the turbulent boundary layer thickness of a plate can be calculated using the following formula:

$$\begin{cases} Re(l) = ul/\nu, \\ \Delta y(l) > 4.4456\times10^{-5} Re(l)^{1/8}, \\ \Delta y(l) < 4.4456\times10^{-4} Re(l)^{1/8}, \end{cases} \tag{7}$$

where $Re(l)$ is the Reynolds number of a plate with the length of l, and $\Delta y(l)$ is the turbulent boundary layer thickness of a plate with the length of l.

In a 10:1 vehicle body model, the length of engine cover lid is $l_F=0.116$ m and the length of body cap is $l_T=0.134$ m. When the velocity $u=30$ m/s, it can be calculated that:

$$\begin{cases} 0.2068\text{ mm} < \Delta y(l_F) < 2.068\text{ mm}, \\ 0.2105\text{ mm} < \Delta y(l_T) < 2.105\text{ mm}. \end{cases} \tag{8}$$

The results indicate that in a vehicle body model with 10:1 ratio, the height or depth of non-smooth units at the engine cover lid should be set between 0.2068 and 2.068 mm and the height or depth of non-smooth units at the body cap should be set from 0.2105 to 2.105 mm.

3 Models used for analysis

The vehicle outflow field is defined by a series of characteristics such as its viscosity, incompressibility, isothermality, and stability. In addition to the regular laminar flow, the turbulent flow is also found in the vehicle outflow field, and it has been demonstrated that the turbulent flow, especially when it is featured with wall-bounded constraint, has significant impacts on the vehicle outflow field.

1. The realizable k-ε turbulence model (Launder and Spalding, 1974) with modifications according to the standard wall function was used in this study.

2. The computational domain input was set to be the speed which was given as u=30 m/s. The computational domain output was set to be pressure and relatively the pressure of the inflow in distance was given as P=0 (Pa). The bottom, sides, and top boundaries of the computational domain, and the boundary of the vehicle body model, were all fixed.

3. SIMPLC algorithm was used as the solution method. The turbulent kinetic energy and turbulent kinetic energy dissipation rate were all set as second order upwind form. The turbulent kinetic energy is given as $k=3/2(uI)^2$, and the energy dissipation rate is given as $\varepsilon=C_\mu^{3/4}(k^{3/2}/l)$. The sub-relaxation factor was set in accordance with the requirements.

4. The CAD model of a vehicle body with 10:1 ratio was constructed as shown in Fig. 2 (Zhang, 2010). The model is 4430 mm in length, 1900 mm in width, and 1250 mm in height. A wind tunnel, of which the size is eight times longer, six times wider, and six times higher than the model, was placed around the vehicle model. The model, where the wheels were touching the tunnel floor, was placed in the third vehicle model length along the midline of the tunnel facing to the inlet. FLUENT, a computational fluid dynamics (CFD) software (Fluent Inc., 2006), was used to analyze the aerodynamic characteristic, while Hypermesh, a CAE software powered with efficient mesh process ability, was used as a mesh generation tool.

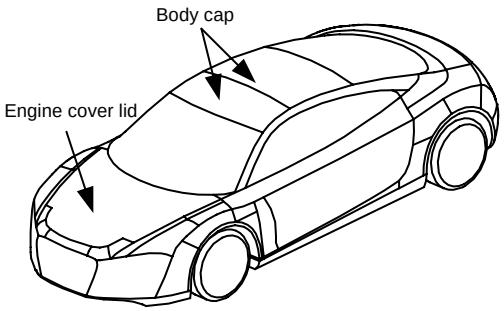

Fig. 2 CAD model of vehicle body

5. The aerodynamic drag coefficient of the car with smooth surfaces was obtained as C_d=0.3197. Compared with the drag coefficient C_d obtained from wind tunnel tests with real vehicles such as Cruze, Lavida, and other comparable cars, the error range was within ±4% since the reported experimental value of drag coefficient resides in the range between 0.31 and 0.33 (Hu, 2009).

4 Simulation tests with non-smooth surfaces

The engine cover lid and vehicle body cap were treated with non-smooth structure units containing pits with the sizes and spacing shown below in Table 1. The pits were in hemispherical shape, of which the width D (mm) is twice the depth H (mm) in size. Pits were uniformly distributed with the horizontal spacing of S (mm) and the vertical distance of L (mm).

Table 1 Drag simulation test for vehicles with bionic non-smooth surfaces containing pits

Code	Engine cover lid		Code	Body cap	
	Spacing, $S\times L$ (mm×mm)	H (mm)		Spacing, $S\times L$ (mm×mm)	H (mm)
F1	12×12	0.75	T1	15×15	1.5
F2	9×9	1.0	T2	12×12	1.5
F3	9×9	0.75	T3	12×12	0.75
F4	6×6	1.0	T4	9×9	1.5
F5	6×6	0.4	T5	9×9	0.75

S: horizontal distance; L: vertical distance; H: height

The vehicle body cap was also treated with non-smooth units containing grooves with the sizes and spacing shown in Table 2, in which d (mm) and h (mm) represent the width and height of the unit, respectively. Again, the units were uniformly distributed with spacing of s (mm).

The aerodynamic drag coefficient of a vehicle can be calculated by the simulation model, and the drag reduction rate R_d can be calculated as

$$R_d=\frac{C_d^S-C_d^T}{C_d^S}\times 100\%, \tag{9}$$

Table 2 Drag simulation test for vehicle body cap with bionic non-smooth surfaces containing grooves

Code	*s*	*d*	*h*	Code	*s*	*d*	*h*
G1	12	2.0	1.0	G7	6	1.0	0.5
G2	12	1.0	1.0	G8	6	0.6	1.2
G3	9	1.0	2.0	G9	6	0.6	0.6
G4	9	1.0	1.0	G10	6	0.6	0.3
G5	6	1.0	2.0	G11	3	0.6	0.6
G6	6	1.0	1.0	G12	3	0.6	0.3

s: horizontal distance, mm; *d*: width, mm; *h*: height, mm

where C_d^S is the aerodynamic drag coefficient of a vehicle with smooth surfaces, and C_d^S =0.3197 based on the previous analysis, and C_d^T is the aerodynamic drag coefficient of a vehicle with bionic non-smooth surfaces. R_d is positively correlated with drag reduction, namely a bigger R_d indicates better drag reduction. Therefore, R_d<0 indicates that non-smooth units increase the aerodynamic drag coefficient and have no impact on drag reduction.

The results illustrated in Figs. 3–5 show that simulations coded F1, F4, T2, G2, G7, and G12 gave rise to meaningful reduction effects. In contrast, F3 and G9 had no effects, and the rest resulted in insufficient drag reduction. Although the heights or depths of all the units were designed in principle to meet required drag reduction value, the simulation test results showed that not all the units had effects on drag reduction. The possible underlying reason will be discussed and analyzed below to validate the rationality of this method.

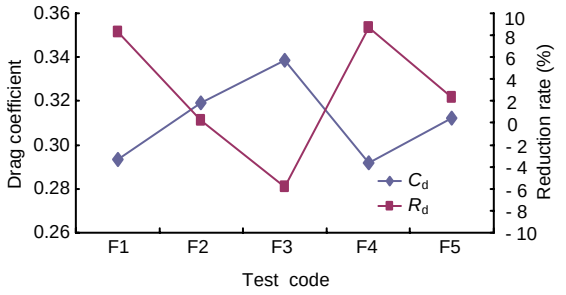

Fig. 3 Drag reduction after the treatment on engine cover lid with bionic non-smooth units containing pits

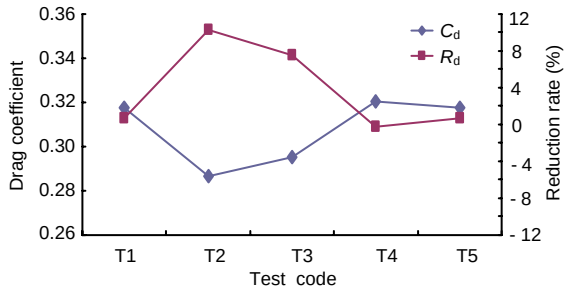

Fig. 4 Drag reduction after the treatment on body cap with bionic non-smooth units containing pits

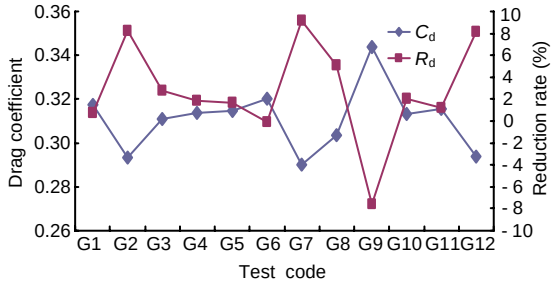

Fig. 5 Drag reduction after treatment on body cap with bionic non-smooth units containing grooves

5 Result analysis in comparison with smooth surface

To better understand the influence of non-smooth surfaces on vehicle aerodynamic performance, we attempted to uncover the mechanism underlying non-smooth surface mediated drag reduction by comparing the effects of non-smooth surface with smooth surface.

The positions of sampling sections were defined according to Fig. 6, in which the vehicle model is placed in the third vehicle length of the wind tunnel facing to the inlet. The size of the car and the tunnel are defined as the simulation model mentioned before. The 1st section is positioned on the very back end of the car that is 1329 mm away from the inlet and 2215 mm away from the outlet. The 2nd to 5th sections are positioned in a sequential order with a 5 mm interval between two adjacent positions, whereas the space between the 5th and the 6th sections is 10 mm.

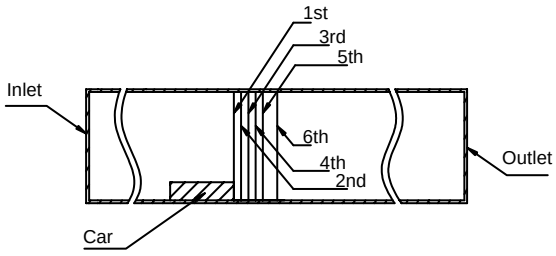

Fig. 6 Positions of sampling sections

Since T2 and G7 caused robust drag reduction in the above simulation tests (Figs. 3–5), these two cases were chosen to compare with the effects of smooth surface. In case one, the non-smooth coded T2, the body cap was treated with pit-containing units with parameters of horizontal spacing S=12.0 mm, vertical spacing L=12.0 mm, and depth H=1.5 mm, the drag coefficient is C_d=0.2867, and the drag reduction rate is 10.31%. In case two, the non-smooth coded G7, the treatment of body cap with the units containing grooves with parameters of spacing s=6.0 mm, width d=1.0 mm, and height h=0.5 mm gave rise to a drag coefficient of C_d=0.2903 and a drag reduction rate of 9.20%.

The air velocity and the turbulence energy distribution at several sections of the rear end of the vehicle body are illustrated in Figs. 7 and 8. As shown in Fig. 7, the air velocities of smooth body at the 1st and 2nd sections were evidently higher than the two non-smooth cases, whereas no significant differences were observed at the 3rd section. Moreover, the situation was reversed at the 4th, 5th, and 6th sections, where the non-smooth body gave higher air velocities.

Fig. 8 compares the distribution of turbulence energy of smooth and non-smooth surfaces at the same back sections. For section 1, the turbulence energy dissipation of the smooth body around part A (labeled in S-k-1st) was evidently larger than the counterparts of the two non-smooth bodies. However, the situation was reversed around parts B or C. This phenomenon also applies to the rest sections. Comparison of the turbulence energy dissipation at part B or C at the 6th section revealed that the turbulence energy dissipation of non-smooth coded T2 was obviously larger than non-smooth coded G7 and the one with smooth surface.

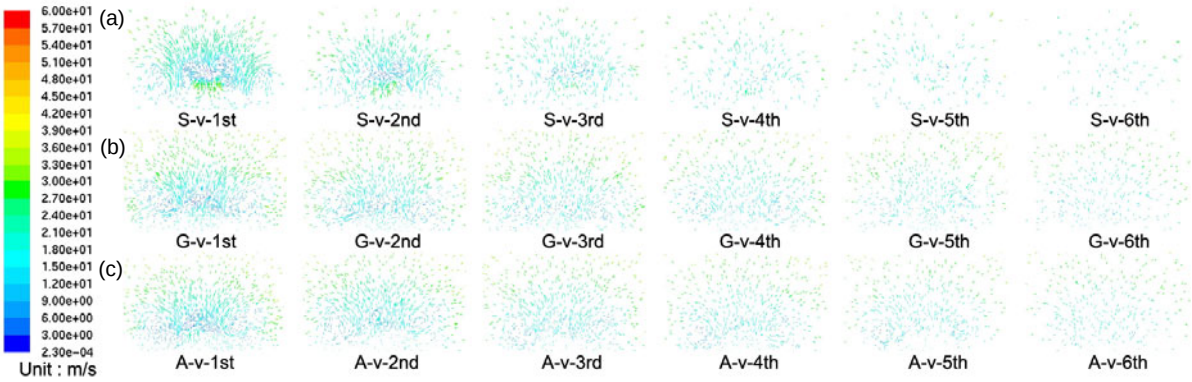

Fig. 7 Distribution of the velocity at six sections behind the back of the vehicle

(a) Vehicle with smooth surfaces; (b) Vehicle with non-smooth unit coded G7; (c) Vehicle with non-smooth unit coded T2. S-v-1st, G-v-1st, and A-v-1st represent distributions of velocity vector at the 1st section of the vehicle with smooth surface, G7, and T2, respectively, and so forth, for sections 2–6

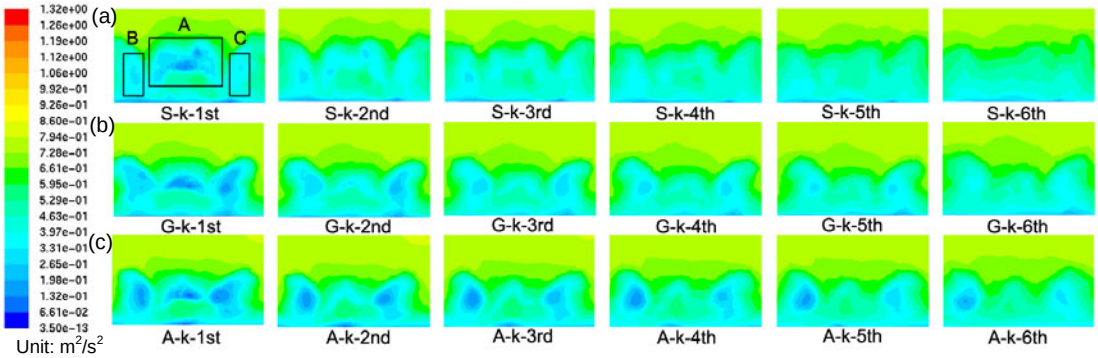

Fig. 8 Distribution of turbulence energy at six sections behind the back of the vehicle

(a) Vehicle with smooth surfaces; (b) Vehicle with non-smooth unit coded G7; (c) Vehicle with non-smooth unit coded T2. S-k-1st, G-k-1st, and A-k-1st represent distributions of turbulence energy at the 1st section of the vehicle with smooth surface, G7, and T2, respectively, and so forth, for sections 2–6

Examination of the distribution of velocity vector and turbulence energy at the back of the vehicle body revealed that the speed of the airflow from the top to the back of the vehicle body was enhanced after the non-smooth unit was introduced and the airflow was also able to move longer after breaking away from the back of the vehicle. The merge of the airflows from the top and the sides of the body resulted in a new merged velocity that enhances the dissipation at part B or C, but weakens the dissipation at part A. With the increase of the pressure over the core area, labeled as A, on the back of the vehicle, the pressure drag of the vehicle decreases, leading to the desired vehicle aerodynamic drag reduction and a lower C_d value. How non-smooth units reduce the friction between the airflow and the top surface of the vehicle to enhance the airflow velocity remains an open question and requires further study.

6 Discussion and conclusions

It appears that both the structure and size of the non-smooth unit can influence drag reduction. Additional theoretical studies are required for further improvements in bionic non-smooth design. Itoh *et al.* (2006) tested the drag-reducing ability of the seal fur surface in a rectangular channel flow using both water and glycerol-water mixture. They measured the pressure drop along the channel in order to evaluate friction factors under various conditions with a wide range of Reynolds number and the drag reduction effect was recorded quantitatively. The maximum reduction ratio was found to be 12% for the glycerol-water mixture, and the stream wise turbulence intensity for the seal fur surface was about 5% lower than the ones with smooth and riblet surfaces. Brucker and Keissner (2010) applied cilia bundles onto the surfaces as passive structures for the near-wall control of boundary layer flows. The micro-pillar arrays are arranged in the form of a V bundle shape often found in natural environment. Although the micro-pillars (diameter D=50 and 100 μm) with specific parameters have a good effect on near-wall control, no interpretation has yet been given regarding how it works.

A new approach to reduce the aerodynamic drag coefficient by attaching bionic non-smooth surfaces on motor vehicle body was proposed in our previous study (Song *et al.*, 2010) and is elaborated in the current study. Based on our analysis of the mechanisms underlying non-smooth surface mediated drag reduction as well as the prevailing model speculating that the drag reduction is largely achieved through controlling the boundary layer to reduce the burst and the loss of turbulent kinetic energy, we designed the non-smooth units containing pits and grooves with suitable size range to fully adapt the structure of a given vehicle body surface. As to the location of the units, engine cover lid and vehicle body cap were chosen, as examples, to host to the units in this initial study. The simulation results showed that when the vehicle speed reaches 30 m/s, a drag reduction rate up to 10.31% is observed, confirming the feasibility of vehicle aerodynamic drag reduction by this new bionic non-smooth surface based approach. These results provide significant insights into drag reduction of motor vehicle and will stimulate further studies in the field.

References

Bourisli, R.I., Al-Sahhaf, A.A., 2008. CFD Modeling of Turbulent Boundary Layer Flow in Passive Drag-Reducing Applications. Advances in Fluid Mechanics VII, WIT Transactions on Engineering Science, **59**:79-90. [doi:10.2495/AFM080081]

Brucker, C., Keissner, A., 2010. Streaming and mixing induced by a bundle of ciliary vibrating micro-pillars. *Experiments in Fluids*, **49**(1):57-65. [doi:10.1007/s00348-009-0774-7]

Bullen, R.D., McKenzie, N.L., 2008. The pelage of bats (Chiroptera) and the presence of aerodynamic riblets: the effect on aerodynamic cleanliness. *Zoology*, **111**(4):279-286. [doi:10.1016/j.zool.2007.09.001]

Choi, K.S., 2006. Fluid dynamics-the rough with the smooth. *Nature*, **440**:754. [doi:10.1038/440754a]

EI-Samni, O.A., Yoon, H.S., Chun, H.H., 2005. Turbulent flow over thin rectangular riblets. *Journal of Mechanical Science and Technology*, **19**(9):1801-1810.

EI-Samni, O.A., Chun, H.H., Yoon, H.S., 2007. Drag reduction of turbulent flow over thin rectangular riblets. *International Journal of Engineering Science*, **45**(2-8):436-454. [doi:10.1016/j.ijengsci.2007.03.002]

Fluent Inc., 2006. FLUENT User's Guide. Available from http://my.fit.edu/itresources/manuals/fluent6.3/help/html/ug/main_pre.htm [Accessed on June 10, 2011]

Fransson, J.H.M., Talamelli, A., Brandt, L, Cossu, C., 2006. Delaying transition to turbulence by a passive mechanism. *Physical Review Letters*, **96**(6):064501. [doi:10.1103/PhysRevLett.96.064501]

Fu, L.M., Cai, G.H., 1998. Testing research in wind tunnel for reducing the drag force acting on the home-made car. *Acta Aerodynamica Sinica*, **16**(2):147-153 (in Chinese).

Gad-el-Hak, M., 2006. Compliant Coatings: The Simpler Alternative. 13th Workshop on Transition and Turbulence Control, Institute for Mathematical Sciences, National University of Singapore, Singapore, **8**:357-404. [doi:10.1142/9789812700896_0012]

Gu, Z.Q., Li, X.W., He, Y.B., 2008. A new method of reducing aerodynamic drag. *Automotive Engineering*, **30**(5):441-448 (in Chinese).

Hu, Y.P., 2009. An Inventory of Thirteen Compact-Car's Drag Coefficient. Available from http://www.autohome.com.cn/advice/201104/67567-3.html (in Chinese) [Accessed on Apr. 3, 2011]

Itoh, M., Tamano, S., Iguchi, R., Yokota, K., Akino, N., Hino, R., Kubo, S., 2006. Turbulent drag reduction by the seal fur surface. *Physics of Fluids*, **18**(6):065102. [doi:10.1063/1.2204849]

Koike, M., Nagayoshi, T., Hamamoto, N., 2004. Research on Aerodynamic Drag Reduction by Vortex Generators. Mitsubishi Motors Technical Review, p.11-16.

Launder, B.E., Spalding, D.B., 1974. The numerical computation of turbulent flows. *Computer Methods in Applied Mechanics and Engineering*, **3**(2):269-289. [doi:10.1016/0045-7825(74)90029-2]

Nisugi, K., Hayase, T., Shirai, A., 2004. Fundamental study of aerodynamic drag reduction for vehicle with feedback flow control. *JSME International Journal Series B*, **47**(3):584-592. [doi:10.1299/jsmeb.47.584]

Ren, L.Q., Zhang, C.C., Tian, L.M., 2005. Experimental study on drag reduction for bodies of revolution using bionic non-smoothness. *Journal of Jilin University (Engineering and Technology Edition)*, **35**(4):431-436 (in Chinese).

Salari, K., 2006. Heavy Vehicle Drag Reduction Devices: Computational Evaluation & Design. Department of Energy Heavy Vehicle Systems Review, USA.

Singh, S.N., Rai, L., Puri, P., Bhatnagar, A., 2005. Effect of moving surface on the aerodynamics drag of road vehicles. *Proceedings of the Institution of Mechanical Engineers, Part D: Journal of Automobile Engineering*, **219**(2):127-134. [doi:10.1243/095440705X5886]

Sirovich, L., Karlsson, S., 1997. Turbulent drag reduction by passive mechanisms. *Nature*, **388**(6644):753-755. [doi:10.1038/41966]

Song, X.W., Zhang, G.G., Wang, Y., Hu, S.G., 2010. Aerodynamic drag reduction analysis of vehicle body with bionic non-smooth surfaces. *Journal of Hunan University (Natural Sciences)*, **37**(12):60-64 (in Chinese).

Tong, J., Moayad, B.Z., Ma, Y.H., Sun, J.Y., Chen, D.H., Jia, H.L., Ren, L.Q., 2009. Effects of biomimetic surface designs on furrow opener performance. *Journal of Bionic Engineering*, **6**(3):280-289. [doi:10.1016/S1672-6529(08)60128-6]

Versteeg, H.K., Malalasekera, W., 1995. An Introduction to Computational Fluid Dynamics: The Finite Volume Method. Wiley, New York, USA.

Walsh, M.J., Sellers, W.L., McGinley, C.B., 1989. Riblet drag reduction at flight conditions. *Journal of Aircraft*, **26**(6):570-575. [doi:10.2514/3.45804]

Wang, F.J., 2004. Computational Fluid Dynamics: Principle and Application of CFD Software. Tsinghua University Press, Beijing, China, p.125-132 (in Chinese).

Whitmore, S.A., Naughton, J.W., 2002. Drag reduction on blunt-based vehicles using forebody surface roughness. *Journal of Spacecraft and Rockets*, **39**(4):596-604. [doi:10.2514/2.3849]

Zhang, C.C., 2007. Drag Reduction of Bodies of Revolution by Flow Control Using Bionic Non-Smooth Surface. MS Thesis, Jilin University, Changchun, China (in Chinese).

Zhang, G.G., 2010. Research on Aerodynamic Drag Reduction of Vehicle Body with Bionic Non-smooth Surfaces. MS Thesis, Zhejiang University, Hangzhou, China (in Chinese).

Zhou, C.H., Tian, L.M., Ren, L.Q., Zhao, W.F., Zhang, R., Zhang, S.C., 2006. Research on non-smooth surface morphology and bionic technology of Columba livia feather. *Transactions of the Chinese Society for Agricultural Machinery*, **37**(11):180-183 (in Chinese).